A Sequential SISO Stability Analysis Model for Grid-Connected Converters by Considering the Impact of Power Flow Direction

Haitao Zhang, *Member, IEEE*, Maryam Saeedifard, *Fellow, IEEE*, Xiuli Wang, *Senior Member, IEEE*, Fengting Wei, *Graduate Student Member, IEEE*, and Xifan Wang, *Life Fellow, IEEE*

***Abstract*—For grid-connected converters operating under nonunity power factor, their dq admittances become off-diagonal due to emerging of the coupling admittances. Consequently, the grid-connected converter systems become multi-input multioutput (MIMO) systems whose stability analysis becomes challenging. To avoid the multivariable nature for system stability analysis, by considering the impact of power flow direction and converter admittance characteristics, this article formulates a sequential single-input single-output (SISO) stability analysis model for grid-connected converter systems. Compared with the existing SISO models, the proposed one offers salient features as follows. 1) Different power flow directions correspond to different stability analysis sequences and system minor-loop gains. 2) It possesses a more clear physical meaning and explicitly identifies the contributions of different parts, including the d-axis subsystem, the coupling of the d-axis subsystem with the q-axis subsystem, and the q-axis subsystem to the system stability. 3) The proposed system minor-loop gain never contains any RHP pole and therefore, the system stability analysis and oscillation mechanism illustration are greatly simplified. Furthermore, the classical control theory can be introduced to guide the system analysis and design. Simulation results are presented to validate the accuracy of the proposed sequential SISO model.**

***Index Terms*—dq admittance model, grid-connected converter system, harmonic stability, single-input single-output (SISO).**

Manuscript received 16 April 2023; revised 15 July 2023 and 13 September 2023; accepted 18 September 2023. Date of publication 14 December 2023; date of current version 26 January 2024. This work was supported in part by the Fundamental Research Funds for the Central Universities under Grant xzy012021016, in part by the State Key Laboratory of Electrical Insulation and Power Equipment under Grant EIPE22308, in part by the Shaanxi Provincial Natural Science Basic Research Program Youth Project under Grant 2022JQ-309, in part by the China Postdoctoral Science Foundation under Grant 2022M712512, and in part by the National Natural Science Foundation of China under Grant 52207137. Recommended for publication by Associate Editor F. J. Azcondo. *(Corresponding author: Haitao Zhang.)*

Haitao Zhang, Xiuli Wang, Fengting Wei, and Xifan Wang are with the State Key Laboratory of Electrical Insulation and Power Equipment, School of Electrical Engineering, Xi'an Jiaotong University, Xi'an 710049, China (e-mail: htzhangee@gmail.com; xiuliw@mail.xjtu.edu.cn; ftwei@stu.xjtu.edu.cn; xfwang@mail.xjtu.edu.cn).

Maryam Saeedifard is with the School of Electrical and Computer Engineering, Georgia Institute of Technology, Atlanta, GA 30332 USA (e-mail: maryam@ece.gatech.edu).

Color versions of one or more figures in this article are available at https://doi.org/10.1109/TPEL.2023.3343353.

Digital Object Identifier 10.1109/TPEL.2023.3343353

I. Introduction

In recent years, the massive integration of grid-connected converters and energy storage devices [1], [2], [3] has created significant concerns over system harmonic stability analysis [4], [5]. As such two methods including the impedance-based method [6], [7], [8] and the state–space method [9], [10], [11] have been commonly used for harmonic stability analysis. Compared with the state–space method, the former one does not involve high-order differential equations [12] and possesses a clear physical meaning [13]. What is more, as only the externally measured impedances (or admittances) are utilized in the system stability assessment, the impedance-based analysis method offers advantages in protecting intellectual property [14] and is widely used in the existing studies.

Corresponding to the impedance-based analysis method, three different admittance models, including the dq admittance model [15], [16], the sequence admittance model [17], [18], [19], and the symmetric admittance model [20] are formulated in the dq synchronous reference frame, the phasor domain, and the polar frame, respectively. Regarding the dq admittance model, when converters operate under unity power factor, their dq admittance model degrades into a diagonal matrix since the coupling admittances are negligible [16]. Given that the coupling impedances of the ac grid are pretty small, the system stability can be analyzed approximately through two single-input single-output (SISO) models. Such a practice simultaneously facilitates the system integration and design and greatly simplifies the system stability analysis. However, when the steady-state operation points of converters deviate from the unity power factor, the coupling admittances become nonnegligible anymore [15]. Under this condition, the system stability cannot be judged intuitively from impedance interactions like what has been done in the dc systems, as it depends, instead, on the eigenvalues of high order matrices, which makes the mechanism of system instability challenging and less clear to grasp. The sequence admittance model has similar characteristics [21]. As has been pointed out by [22], [23], the coupling admittances of the positive sequence with the negative sequence cannot be neglected though their magnitudes are very small. Neglecting the small coupling term will result in a false estimation of the system stability. In conclusion, due to the existence of coupling admittances, grid-tied converter systems are essentially multi-input multioutput (MIMO) systems and

the general Nyquist criterion (GNC) becomes inevitable [24], [25]. Although the result is accurate, the adoption of the GNC complicates the stability analysis and oscillation mechanism illustration. Therefore, the system stability analysis based on a SISO model charges this.

To avoid the multivariable nature and address the complexity of stability analysis for MIMO systems, various SISO models have been developed for single-phase and three-phase grid-connected converters, microgrids, and large-scale power systems [20], [26], [27], [28], [29], [30], [31], [32], [33], [34], [35], [36], [37], [38], [39], [40], [41], [42]. The commonly used approach is based on pure matrix operations, which decouples the original MIMO system into two SISO sequence impedance-based models [26], [27], [28]. Although this technique successfully avoids the need for the GNC, it may introduce right-half plane (RHP) poles into the system's minor-loop gain [29]. In such cases, the proposed SISO model may face challenges when it comes to illustrating the oscillation mechanism and conducting system analysis and design. In an effort to eliminate possible RHP poles, researchers have constructed a single SISO model based on a symmetric admittance model [20]. However, this approach heavily relies on the symmetrical characteristics of converter admittances, making it vulnerable to changes in control strategies or power factors. Apart from the pure matrix operation, another method known as the transfer function method has been introduced to derive SISO models for single-phase grid-connected converters [30], [31], three-phase grid-connected converters [32], [33], [34], [35], microgrids [36], and VSC-HVDC systems [37]. However, this method has limitations as it requires detailed information about the converter's internal physical structure and parameters, and it fails to consider the impact of time delays introduced by digital control. In addition to these methods, several alternative approaches have been formulated, including the Gershgorin theorem-based SISO model [38], the eigenvalue decomposition-based SISO model [39], the recursive SISO model [40], the decoupling control-based SISO model [41], and the decoupled voltage amplitude/phase dynamic SISO model [42]. However, none of these methods successfully achieve the following objectives simultaneously.

1) Avoiding the need for information regarding the system's internal physical structure and parameters, thereby effectively safeguarding intellectual property.
2) Streamlining system stability analysis and distinguishing between various sources of instability.
3) Offering clear physical interpretations that elucidate the underlying oscillation mechanism.

To address the abovementioned issues, by considering the impact of power flow direction and converter admittance characteristics, this article formulates a sequential SISO system stability assessment model based on the dq admittance model. By comparing with the existing SISO models, the proposed sequential SISO model possesses a more clear physical meaning and offers advantages in identifying the contribution of different parts, including the d-axis subsystem, the coupling of the d-axis subsystem with the q-axis subsystem, and the q-axis subsystem. Furthermore, by guaranteeing that the proposed system minor-loop gain never includes any RHP pole, the Nyquist plot of stable grid-connected converter systems will never encircle $(-1, j0)$ point, which facilitates the system analysis and design via the classical control theory. Table I provides the comparison results of the abovementioned SISO models.

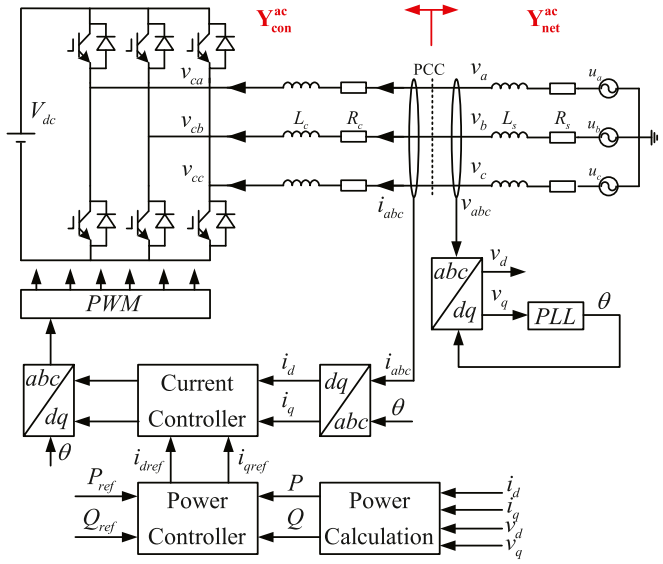

Fig. 1. Main circuit of a grid-connected converter controlled in PQ mode.

The rest of this article is organized as follows. Corresponding to different power flow directions and power factors. Section II investigates the characteristics of the converter dq admittances. Section III formulates the sequential SISO system stability assessment model by considering the impact of power flow directions. Section IV verifies the accuracy of the proposed model with simulations in the MATLAB/Simulink. Finally, Section V concludes this article.

II. Analysis of Dq Admittance Characteristics With Different Power Flow Directions

Converter admittance characteristics lay the foundation for the formulation of the sequential SISO system stability analysis model. By considering the impact of power flow direction, this section first analyzes the converter dq admittance characteristics corresponding to the PQ control mode. The other conditions, i.e., the grid-connected converter operating under other control modes are discussed in Section III-C. Fig. 1 demonstrates the main circuit of a grid-connected converter controlled in PQ mode. As illustrated by Fig. 1, v_{abc} represents the three-phase voltages of the common coupling point (PCC). i_{abc} denotes the currents and its reference direction is indicted by the arrows. By transforming v_{abc} and i_{abc} into the dq synchronous reference frame, their d-axis (q-axis) components are labeled as $v_d(v_q)$, and $i_d(i_q)$, respectively. Then, the power injected by the converter is calculated as

$$P = 1.5(v_d i_d + v_q i_q) \tag{1}$$

$$Q = 1.5(-v_d i_q + v_q i_d) \tag{2}$$

By considering the steady-state value of v_q as 0, setting the small-signal perturbations of P and Q as 0, and linearizing the

TABLE I
COMPARISON OF DIFFERENT SISO MODELS

	The sequence admittance-based model	The symmetric admittance-based model	The transfer function-based model	The Gershgorin -based model	The eigenvalue decomposition-based model	The recursive-based model	The control-based model	The sequential-based model
Sensitivity to the control structure	No	Yes	No	No	No	No	Yes	No
Applicable on one-phase or three-phase converter	Three-phase	Three-phase	Three-phase	Three-phase	Three-phase	One-phase	Three-phase	Three-phase
Clear physical illustration of oscillation mechanism	Yes	Yes	No	No	No	No	No	Yes
Classification of different instability root causes	No	Yes	No	No	No	No	No	Yes
Applicable on pure black-box models	No	Yes	No	Yes	Yes	Yes	No	Yes
References	[26]-[28]	[29]-[30]	[31]-[38]	[39]	[40]	[41]	[42]-[43]	This paper

right-hand sides of (1) and (2), the small-signal representations of (1) and (2) are expressed by

$$\begin{bmatrix}0\\0\end{bmatrix}=\frac{3}{2}\begin{bmatrix}V_d & 0\\0 & -V_d\end{bmatrix}\begin{bmatrix}\tilde{i}_d\\\tilde{i}_q\end{bmatrix}+\frac{3}{2}\begin{bmatrix}I_d & I_q\\-I_q & I_d\end{bmatrix}\begin{bmatrix}\tilde{v}_d\\\tilde{v}_q\end{bmatrix} \tag{3}$$

where V_d and $I_d(I_q)$ denote the steady-state values of v_d and $i_d(i_q)$ while $\tilde{v}_d(\tilde{v}_q)$ and $\tilde{i}_d(\tilde{i}_q)$ stand for the small-signal representations of $v_d(v_q)$ and $i_d(i_q)$, respectively. Based on (3), the converter admittance, i.e., $\mathbf{Y}_{\mathbf{con}}^{ac}$ within the low-frequency range is obtained as

$$\mathbf{Y}_{\mathbf{con}}^{ac}=\begin{bmatrix}-I_d/V_d & -I_q/V_d\\-I_q/V_d & I_d/V_d\end{bmatrix}. \tag{4}$$

Accordingly, the d- and q-axis converter admittances, i.e., Y_{dd}^c and Y_{qq}^c within the low-frequency range are expressed by

$$Y_{dd}^c=-I_d/V_d \tag{5}$$

$$Y_{qq}^c=I_d/V_d. \tag{6}$$

As observed from (5) and (6), the polarity of the d-axis current I_d, i.e., the flow direction of the active power dominates the characteristics of the d- and q-axis converter admittances within the low-frequency range. To be more specific, when the active power transfers to the ac grid, the d-axis current I_d is negative. On this basis, the d-axis admittance within the low-frequency range shows a positive conductance while the q-axis admittance within the low-frequency range demonstrates a negative conductance. In contrast, when the active power is delivered to the converter, the d-axis current I_d becomes positive. Then, the d-axis admittance within the low-frequency range shows a negative conductance behavior while the q-axis admittance within the low-frequency range demonstrates a positive conductance.

To validate the aforementioned admittance characteristics, the detailed dq admittance model developed in [15] is introduced. Since the characteristics of the coupling admittances, including Y_{dq}^c and Y_{qd}^c do not impact the following SISO modeling process, this section mainly analyzes the characteristics of Y_{dd}^c and Y_{qq}^c. Utilizing the system parameters given in Table II, Fig. 2 presents Bode diagrams of the converter dq admittances with different power factors. With respect to Fig. 1, when the converter operates under PF $=-0.8$, i.e., when the active power is transferred to the ac grid, the phase angle of Y_{dd}^c always stays between $-90°$ and $90°$. In other words, Y_{dd}^c has always a positive conductance.

TABLE II
PARAMETERS OF THE GRID-CONNECTED CONVERTER SYSTEM

Symbol	Description	Value
S_b	Base value of power (kVA)	500
U_b	Base value of voltage (V)	690
L_f	Inductance of the converter filter (p.u.)	0.05
R_f	Resistance of the converter filter (p.u.)	0.05
L_s	Equivalent inductance of the ac grid (p.u.)	0.35
k_{pi}	Proportional gain of the current loop	0.25
k_{ii}	Integral gain of the current loop	20
k_{ppq}	Proportional gain of the power control loop	0.0022
k_{ipq}	Integral gain of the power control loop	0.022

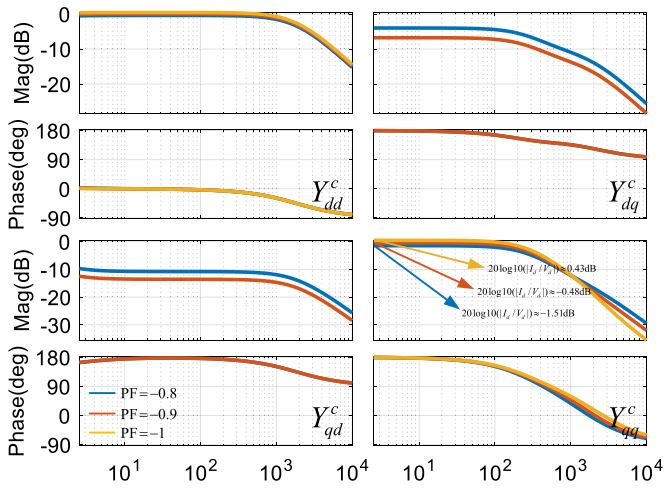

Fig. 2. Bode diagrams of the converter dq admittances with different power factors (PF $=-0.8$, -0.9, and -1).

In contrast, the phase angle of Y_{qq} remains about $-180°$ during the low-frequency range and the magnitude is nearly equal to $20\log_{10}(|I_d/V_d|)=-1.51$ dB, according to the value calculated by (6). With the increase of frequency, the phase angle of Y_{qq}^c decreases and finally drops below $90°$ at about 400 Hz, which signifies that the conductance part of Y_{qq}^c evolves from negative to positive. When the power factor changes from -0.8 to -0.9

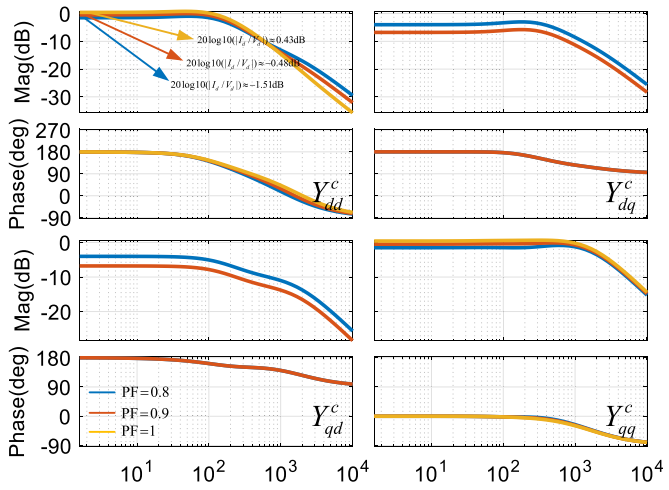

Fig. 3. Bode diagrams of the converter dq admittances with different power factors (PF = 0.8, 0.9, and 1).

TABLE III
PARAMETERS OF THE GRID-CONNECTED CONVERTER SYSTEM

Symbol	Description	Value
S_b	Base value of power (kVA)	500
U_b	Base value of voltage (V)	690
L_f	Inductance of the converter filter (p.u.)	0.05
R_f	Resistance of the converter filter (p.u.)	0.05
L_s	Equivalent inductance of the ac grid (p.u.)	0.35
k_{pi}	Proportional gain of the current loop	0.25
k_{ii}	Integral gain of the current loop	20
k_{ppq}	Proportional gain of the power control loop	0.005
k_{ipq}	Integral gain of the power control loop	0.05

and -1, the dq admittance curves evolve from the blue one to the red and yellow ones, respectively. As illustrated by Fig. 2, the variation of power factor only impacts the numerical values of Y_{dd}^c and Y_{qq}^c while the conductance characteristic remains unchanged. To be more specific, when the active power transfers to the ac grid, the q-axis admittance, i.e., Y_{qq}^c instead of the d-axis admittance, i.e., Y_{dd}^c within the low-frequency range demonstrates a negative conductance behavior.

Once the power flow direction reverses, the Bode diagrams of the converter dq admittances evolve from Figs. 2 to 3. Table III lists the corresponding main parameters. As illustrated in Fig. 3, when the active power is delivered to the converter, the phase angle of Y_{qq}^c is always within the range from $-90°$ and $0°$. Namely, the q-axis admittance, i.e., Y_{qq}^c has always a positive conductance. By comparison, the d-axis admittance, i.e., Y_{dd}^c demonstrates a negative conductance behavior. Specifically, within the low-frequency range, the phase angle of Y_{dd} remains $-180°$. The magnitudes of Y_{dd}^c corresponding to different power factors, including PF = 0.8, 0.9, and 1 are equal to -1.51, -0.48, and 0.43 dB, agreeing with the values calculated by (5). On this basis, when the active power is delivered to the converter, the d-axis admittance, i.e., Y_{dd}^c instead of the q-axis admittance, i.e., Y_{qq}^c within the low-frequency range demonstrates a negative conductance behavior regardless of the power factor.

III. Formulation of the Sequential SISO System Stability Analysis Model

To analyze the system stability, the circuit of Fig. 1 is initially divided into two subsystems from the PCC. The first and second subsystems refer to the ac grid and the converter, respectively. The ac grid dq admittance is denoted by

$$\mathbf{Y}_{\mathbf{net}}^{ac} = \begin{bmatrix} Y_{dd}^s & Y_{dq}^s \\ Y_{qd}^s & Y_{qq}^s \end{bmatrix} \tag{7}$$

where Y_{dd}^s and Y_{qq}^s represent the d- and q-axis ac grid admittances while Y_{dq}^s and Y_{qd}^s denote the corresponding coupling admittances of the d-axis with the q-axis. In addition, without loss of generality, the converter dq admittance corresponding to unity or nonunity power factor is uniformly expressed by

$$\mathbf{Y}_{\mathbf{con}}^{ac} = \begin{bmatrix} Y_{dd}^c & Y_{dq}^c \\ Y_{qd}^c & Y_{qq}^c \end{bmatrix} \tag{8}$$

where Y_{dd}^c and Y_{qq}^c represent the d- and q-axis converter admittances while Y_{dq}^c and Y_{qd}^c denote the corresponding coupling admittances of the d-axis with the q-axis. Assumed that the converter can operate stably and independently, none of the converter admittance elements mentioned in (8) has any RHP pole. Based on the circuit theorem, the characteristic equation is derived as

$$|\mathbf{Y}_{\mathbf{con}}^{ac} + \mathbf{Y}_{\mathbf{net}}^{ac}| = 0 \tag{9}$$

where $|\cdot|$ represents the determinant of a matrix. To analyze the system stability, the key step hinges on identifying whether any poles of the closed-loop system lies on the RHP, i.e., whether the characteristic equation defined by (9) contains any RHP zero. Note that 1) the active power flow direction plays a vital role in the model formulation, and 2) right sequence could greatly simplify the system stability analysis and oscillation mechanism illustration. To clearly illustrate the details, the sequential SISO models corresponding to different power flow directions are studied separately.

A. Sequential SISO System Stability Analysis Model With the Active Power Transferred to the Ac Grid

While the active power is transferred to the ac grid, the q-axis instead of the d-axis converter admittance, i.e., Y_{qq}^c instead of Y_{dd}^c, has a negative conductance [15]. *Under this condition, the d-axis subsystem stability should be assessed first and afterwards, the q-axis subsystem stability is analyzed.* To achieve this goal, the system characteristic equation expressed by (9) is calculated as (10) shown at the bottom of the next page by the properties of determinants. Correspondingly, the grid-connected converter system stability herein fully depends on whether $1 + Y_{dd}^c Y_{dd}^{s-1}$ or $1 + [Y_{qq}^c - (Y_{qd}^s + Y_{qd}^c)(Y_{dd}^s + Y_{dd}^c)^{-1}(Y_{dq}^s + Y_{dq}^c)]Y_{qq}^{s-1}$ contains any RHP zero.

To assess the d-axis subsystem stability, it is equivalent to investigate the number of zeros contained by $1+Y_{dd}^{c}Y_{dd}^{s-1}$. By regarding $1+Y_{dd}^{c}Y_{dd}^{s-1}=0$ as a characteristic equation, the corresponding system minor-loop gain is $Y_{dd}^{c}Y_{dd}^{s-1}$. Notice that 1) neither Y_{dd}^{c} nor Y_{dd}^{s-1} demonstrates any negative conductance and resistor behavior, and 2) neither Y_{dd}^{c} nor Y_{dd}^{s-1} has any RHP pole. The Nyquist plot of $Y_{dd}^{c}Y_{dd}^{s-1}$ will never encircle the point $(-1,j0)$ and $1+Y_{dd}^{c}Y_{dd}^{s-1}$ does not include any RHP zero, which means that the d-axis subsystem stays stable forever. On this basis, the system stability becomes solely hinged on $1+[Y_{qq}^{c}-(Y_{qd}^{s}+Y_{qd}^{c})(Y_{dd}^{s}+Y_{dd}^{c})^{-1}(Y_{dq}^{s}+Y_{dq}^{c})]Y_{qq}^{s-1}$, i.e., the q-axis subsystem stability.

By considering $1+[Y_{qq}^{c}-(Y_{qd}^{s}+Y_{qd}^{c})(Y_{dd}^{s}+Y_{dd}^{c})^{-1}(Y_{dq}^{s}+Y_{dq}^{c})]Y_{qq}^{s-1}=0$ as a characteristic equation, the system minor-loop gain is written as

$$L(s)=[Y_{qq}^{c}-(Y_{qd}^{s}+Y_{qd}^{c})(Y_{dd}^{s}+Y_{dd}^{c})^{-1}(Y_{dq}^{s}+Y_{dq}^{c})]Y_{qq}^{s-1}. \tag{11}$$

Since $1+Y_{dd}^{c}Y_{dd}^{s-1}$ does not include any RHP zero, $(Y_{dd}^{s}+Y_{dd}^{c})^{-1}$ never includes any RHP pole. Besides, as the other terms of $L(s)$, including Y_{qq}^{c}, $(Y_{qd}^{s}+Y_{qd}^{c})$, $(Y_{dq}^{s}+Y_{dq}^{c})$, and Y_{qq}^{s-1} do not contain RHP pole(s) as well, $L(s)$ never include any RHP pole. Therefore, the system stability will be determined by whether the Nyquist plot of $L(s)$ encircles $(-1,j0)$ point and the classical control theory can be introduced to guide system analysis and design. Moreover, the physical meaning of $L(s)$ is clear. Notice that Y_{qq}^{c}, $(Y_{qd}^{s}+Y_{qd}^{c})(Y_{dd}^{s}+Y_{dd}^{c})^{-1}(Y_{dq}^{s}+Y_{dq}^{c})$, and Y_{qq}^{s} represent the q-axis converter admittance, the coupling of the d-axis subsystem with the q-axis subsystem, and the q-axis ac grid admittance, respectively. By regarding $Y_{qq}^{c}-(Y_{qd}^{s}+Y_{qd}^{c})(Y_{dd}^{s}+Y_{dd}^{c})^{-1}(Y_{dq}^{s}+Y_{dq}^{c})$ as the q-axis converter equivalent admittance, $L(s)$ represents the stability correlated with the q-axis subsystem and the coupling of the d-axis subsystem with the q-axis subsystem. The corresponding system stability mechanism can be interpreted as the interaction of the q-axis converter equivalent admittance with the q-axis ac grid admittance. Furthermore, by comparing the relative size of Y_{qq}^{c} and $-(Y_{qd}^{s}+Y_{qd}^{c})(Y_{dd}^{s}+Y_{dd}^{c})^{-1}(Y_{dq}^{s}+Y_{dq}^{c})$, the system instability root causes can be further identified as the q-axis converter admittance or the coupling of the d-axis subsystem with the q-axis subsystem

B. Sequential SISO System Stability Analysis Model With the Active Power Transferred to the Converter

When the active power is transferred to the converter, the d-axis converter admittance, i.e., Y_{dd}^{c}, instead of the q-axis converter admittance, i.e., Y_{qq}^{c}, demonstrates a negative conductance behavior [15]. *Under this new circumstance, the system stability should be analyzed in accordance with the q-axis subsystem and the d-axis subsystem sequence order.* To this end, the characteristic equation expressed by (9) is recalculated as (12) shown at the bottom of this page. According to (12), the system stability relies on whether $1+Y_{qq}^{c}Y_{qq}^{s-1}$ or $1+[Y_{dd}^{c}-(Y_{dq}^{s}+Y_{dq}^{c})(Y_{qq}^{s}+Y_{qq}^{c})^{-1}(Y_{qd}^{s}+Y_{qd}^{c})]Y_{dd}^{s-1}$ contains any RHP zero.

To investigate the q-axis subsystem stability, $1+Y_{qq}^{c}Y_{qq}^{s-1}=0$ is considered as a characteristic equation and the corresponding system minor-loop gain is $Y_{qq}^{c}Y_{qq}^{s-1}$. Since both Y_{qq}^{c} and Y_{qq}^{s-1} do not have any RHP pole and do not contain any negative conductance and resistance, the Nyquist plot of $Y_{qq}^{c}Y_{qq}^{s-1}$ never encircle $(-1,j0)$ point and $1+Y_{qq}^{c}Y_{qq}^{s-1}$ does not include any RHP zero. On this basis, the q-axis subsystem remains stable forever and the system stability becomes solely subject to $1+[Y_{dd}^{c}-(Y_{dq}^{s}+Y_{dq}^{c})(Y_{qq}^{s}+Y_{qq}^{c})^{-1}(Y_{qd}^{s}+Y_{qd}^{c})]Y_{dd}^{s-1}$, i.e., the d-axis subsystem stability.

By regarding $1+[Y_{dd}^{c}-(Y_{dq}^{s}+Y_{dq}^{c})(Y_{qq}^{s}+Y_{qq}^{c})^{-1}(Y_{qd}^{s}+Y_{qd}^{c})]Y_{dd}^{s-1}=0$ as a new characteristic equation, the new system minor-loop gain governing the system stability is defined as

$$L'(s)=[Y_{dd}^{c}-(Y_{dq}^{s}+Y_{dq}^{c})(Y_{qq}^{s}+Y_{qq}^{c})^{-1}(Y_{qd}^{s}+Y_{qd}^{c})]Y_{dd}^{s-1}. \tag{13}$$

Similar to the discussion for $L(s)$, when the active power flow direction reverses, $L'(s)$ never has any RHP pole either. Consequently, the system stability is determined by the relative locations of the Nyquist plot of $L'(s)$ and the critical point $(-1,j0)$. In addition, the physical meaning of $L'(s)$ is also apparent. Notice that Y_{dd}^{c}, $(Y_{dq}^{s}+Y_{dq}^{c})(Y_{qq}^{s}+Y_{qq}^{c})^{-1}(Y_{qd}^{s}+Y_{qd}^{c})$, and Y_{dd}^{s} represent the d-axis converter admittance, the coupling of the d-axis subsystem with the q-axis subsystem, and the d-axis ac grid admittance, respectively. By regarding $Y_{dd}^{c}-(Y_{dq}^{s}+Y_{dq}^{c})(Y_{qq}^{s}+Y_{qq}^{c})^{-1}(Y_{qd}^{s}+Y_{qd}^{c})$ as the d-axis converter equivalent admittance, $L'(s)$ represents the stability of the d-axis subsystem (and the stability correlated with the coupling of the d-axis subsystem with the q-axis subsystem). The system stability mechanism can be explained as the interaction of the d-axis converter equivalent admittance and the d-axis ac grid admittance. In addition, by evaluating the different contributions of Y_{dd}^{c} and $(Y_{dq}^{s}+Y_{dq}^{c})(Y_{qq}^{s}+Y_{qq}^{c})^{-1}(Y_{qd}^{s}+Y_{qd}^{c})$ to the d-axis converter equivalent admittance, the system instability root causes can be further classified into the d-axis converter admittance or the coupling between of the d-axis subsystem with the q-axis subsystem.

C. Sequential SISO System Stability Analysis Model With Converters Controlled in Other Modes

According to Sections III-A and B, the formation of the sequential SISO models strongly correlates with the converter dq admittance characteristics. To verify its universality, the admittance characteristics of the converters controlled in the

$$(1+Y_{dd}^{c}Y_{dd}^{s-1})(1+[Y_{qq}^{c}-(Y_{qd}^{s}+Y_{qd}^{c})(Y_{dd}^{s}+Y_{dd}^{c})^{-1}(Y_{dq}^{s}+Y_{dq}^{c})]Y_{qq}^{s-1})=0 \tag{10}$$

$$(1+Y_{qq}^{c}Y_{qq}^{s-1})(1+[Y_{dd}^{c}-(Y_{dq}^{s}+Y_{dq}^{c})(Y_{qq}^{s}+Y_{qq}^{c})^{-1}(Y_{qd}^{s}+Y_{qd}^{c})]Y_{dd}^{s-1})=0. \tag{12}$$

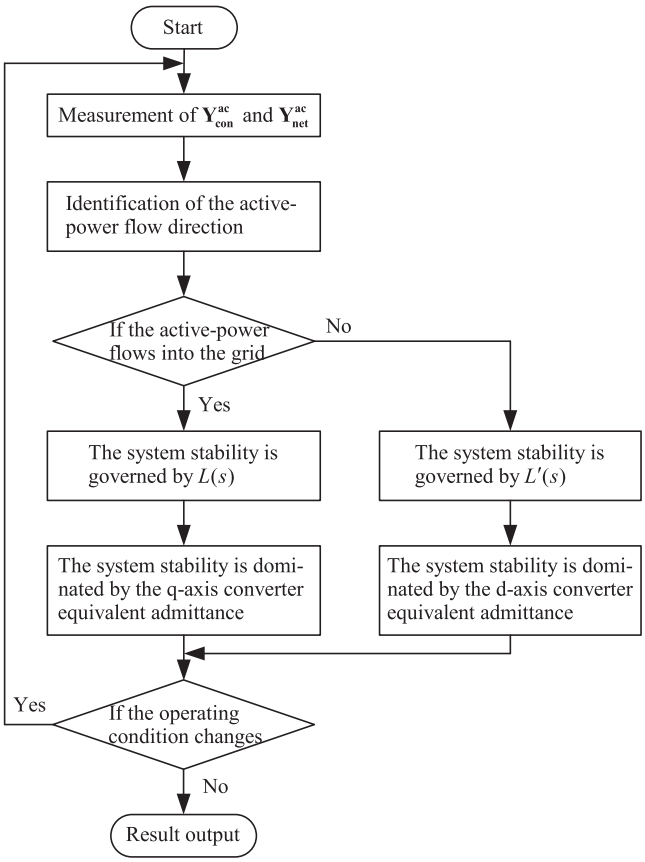

Fig. 4. Flowchart of the proposed sequential SISO model.

current control mode, the dc voltage mode, the droop control mode, and the virtual synchronous control mode are investigated based on the detailed dq admittance models in [15], [16], [43], [44]. The results reveal that the admittance characteristic of the converter controlled in the current or dc voltage mode is similar to or even simpler than the one presented in Section II. For example, when a converter is controlled in the current mode, its q-axis admittance, i.e., Y_{qq} demonstrates a negative conductance behavior when the active power transfers from the converter into the ac grid. Its d-axis admittance, i.e., Y_{dd} only has a positive conductance regardless of the power flow direction. Notice that the d- and q-axis converter admittances will not simultaneously demonstrate a negative conductance behavior. For any certain active power flow direction, only the q- or d-axis converter admittance contains negative conductance. Correspondingly, the d- or q-axis subsystem can be eliminated and the sequential SISO model for the grid-connected converters controlled in other modes can be formulated with similar processes shown in Sections III-A and B. For the sake of clarification, Fig. 4 provides the flowchart of the proposed sequential SISO model. It is worth to note that the proposed SISO model is temporarily applicable for the grid-connected converters and the paralleled converter systems rather than the system-level large scale power electronics-dominated power systems. The SISO model applicable for the system-level large scale power electronics-dominated power systems still needs further investigation in the future.

IV. Simulation

A. System Stability Analysis With the Active Power Transferred to the AC Grid

Utilizing the parameters in Table II, the system in Fig. 1 is simulated. By setting the power factor as -0.8, the Nyquist plot of $L(s)$ is plotted with blue color in Fig. 5(a) while the unit circle is marked by red color. As illustrated by Fig. 5(a), the Nyquist plot intersects with the unit circle at 270 Hz and encircles $(-1, j0)$ point twice. Based on the Nyquist criterion, the system should contain two RHP poles and stay oscillatory. To identify the system instability root causes, Fig. 5(b) presents the Bode diagrams of Y_{qq}^c, $-(Y_{qd}^s+Y_{qd}^c)(Y_{dd}^s+Y_{dd}^c)^{-1}(Y_{dq}^s+Y_{dq}^c)$, and $Y_{qq}^c-(Y_{qd}^s+Y_{qd}^c)(Y_{dd}^s+Y_{dd}^c)^{-1}(Y_{dq}^s+Y_{dq}^c)$, respectively. With respect to Fig. 5(b), the magnitude of Y_{qq}^c is about 20 dB larger than that of $-(Y_{qd}^s+Y_{qd}^c)(Y_{dd}^s+Y_{dd}^c)^{-1}(Y_{dq}^s+Y_{dq}^c)$ around 270 Hz. In other words, the real value of Y_{qq}^c is about ten times larger than that of $-(Y_{qd}^s+Y_{qd}^c)(Y_{dd}^s+Y_{dd}^c)^{-1}(Y_{dq}^s+Y_{dq}^c)$. Therefore, the system instability is triggered by the q-axis converter admittance rather than the coupling of the d-axis subsystem with the q-axis subsystem. To stabilize the grid-connected converter system, the parameters of the q-axis power control loop, i.e., k_{ppq} and k_{ipq} are decreased to 0.002 and 0.02 at $t = 5$ s. Accordingly, the Nyquist plot develops to the orange one. As illustrated by Fig. 5(a), the new Nyquist plot never encircles $(-1, j0)$ point anymore. Consequently, the system is successfully stabilized and the oscillations are effectively mitigated by the parameter tuning at $t = 5$ s, which closely agrees with the time-domain waveform presented by Fig. 5(c). Apart from the converter operating under PF $= -0.8$, Figs. 6(a) and 7(a) study the system stability of grid-connected converters operating under PF $= -0.9$ and PF $= -1$, respectively. The unit circle is marked by red color while the Nyquist plots of $L(s)$ before and after the parameter tuning are plotted with blue and orange colors, respectively. With respect to Figs. 6(a) and 7(a), the Nyquist plots marked by blue color encircle $(-1, j0)$ point twice clockwise and consequently, the grid-connected converter systems are unstable. Furthermore, note that 1) the Nyquist plots of $L(s)$ in Figs. 6(a) and 7(a) interact with the unit circle at 250 and 240 Hz, and 2) the real values of Y_{qq}^c in Figs. 6(b) and 7(b) are much larger than that of $-(Y_{qd}^s+Y_{qd}^c)(Y_{dd}^s+Y_{dd}^c)^{-1}(Y_{dq}^s+Y_{dq}^c)$ around 250 and 240 Hz. The system stabilities for the converter operating under PF $= -0.9$ and PF $= -1$ are still governed by the q-axis converter admittance. Resetting k_{ppq} and k_{ipq} to 0.0016(0.001) and 0.016(0.01), the Nyquist plots of $L(s)$ are represented with orange color in Figs. 6(a) and 7(a). With respect to Figs. 6(a) and 7(a), $(-1, j0)$ point is never encircled by the new Nyquist plots anymore, which means that the system is effectively stabilized. The analysis results accord to the time-domain simulations illustrated by Figs. 6(c) and 7(c). To be more specific, subsequent to the parameters tuning at $t = 5$ s, the oscillations attenuate rapidly and all the variables get back to their normal values.

B. System Stability Analysis With the Active Power Transferred to the Converter

When active power flows from the ac grid into the converter, $L'(s)$ rather than $L(s)$ goes into effect. To validate the

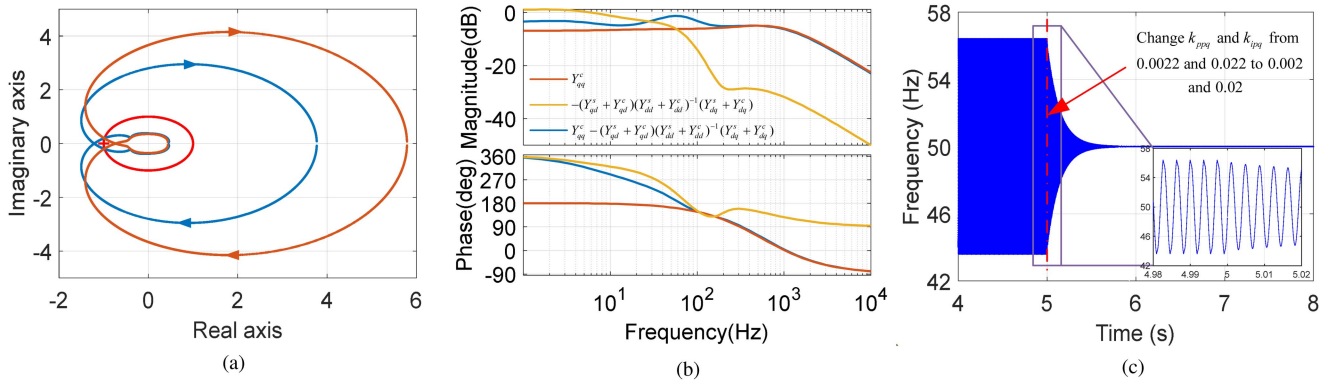

Fig. 5. Case study of the grid-connected converter operating under PF $= -0.8$. (a) Nyquist plots of $L(s)$. (b) Bode diagrams of different admittances. (c) Simulation of the PLL output frequency in the time domain.

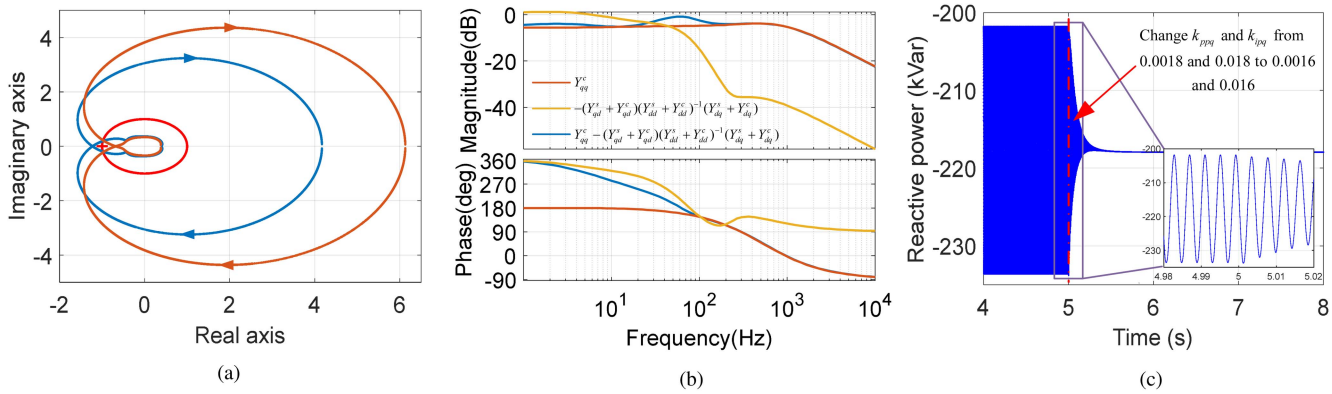

Fig. 6. Case study of the grid-connected converter operating under PF $= -0.9$. (a) Nyquist plots of $L(s)$. (b) Bode diagrams of different admittances. (c) Simulation of the reactive power in the time domain.

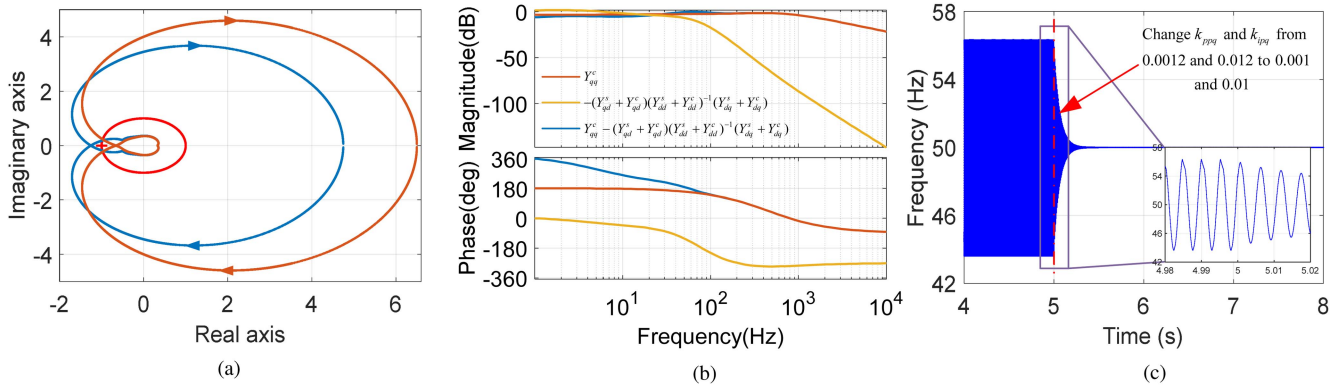

Fig. 7. Case study of the grid-connected converter operating under PF $= -1$. (a) Nyquist plots of $L(s)$. (b) Bode diagrams of different admittances. (c) Simulation of the PLL output frequency in the time domain.

sequential SISO model formulated in Section III-B, a system with the parameters listed in Table III is introduced. When the converter operates under PF $= 0.8$, the Nyquist plot of $L'(s)$ is demonstrated in Fig. 8(a) with blue color. The arrows in Fig. 8(a) indicate the frequency increasing from 0.1 Hz to 10 kHz. As presented by Fig. 8(a), the Nyquist plot never encircles $(-1, j0)$ point and therefore, the system stays stable. By increasing k_{ppq} and k_{ipq} from 0.005 and 0.05 to 0.0052 and 0.052, the Nyquist plot develops to the orange one. As presented by Fig. 8(a), the new Nyquist plot surrounds $(-1, j0)$ point once clockwise and interact with the unit circle at 6000 Hz. Based on the Nyquist criterion, the grid-connected converter system

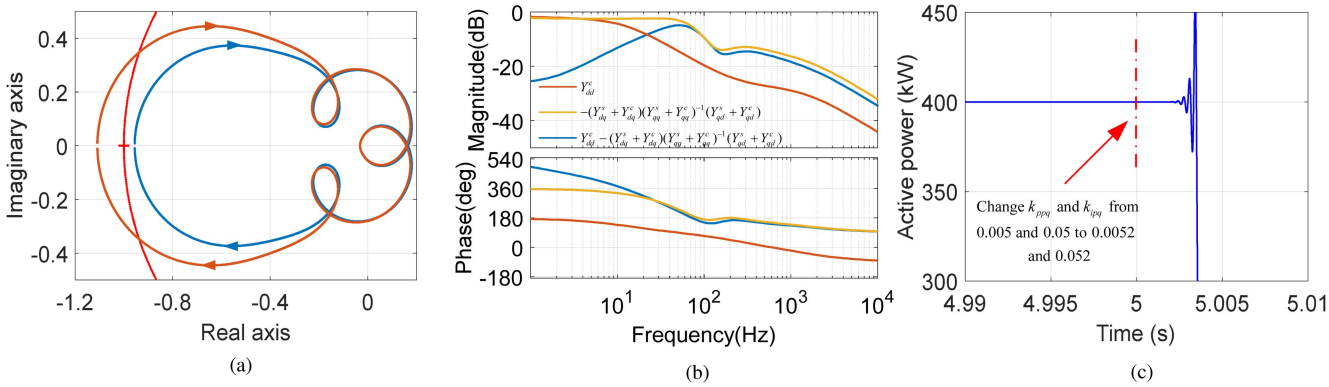

Fig. 8. Case study of the grid-connected converter operating under PF = 0.8. (a) Nyquist plots of $L'(s)$. (b) Bode diagrams of different admittances. (c) Simulation of the active power in the time domain.

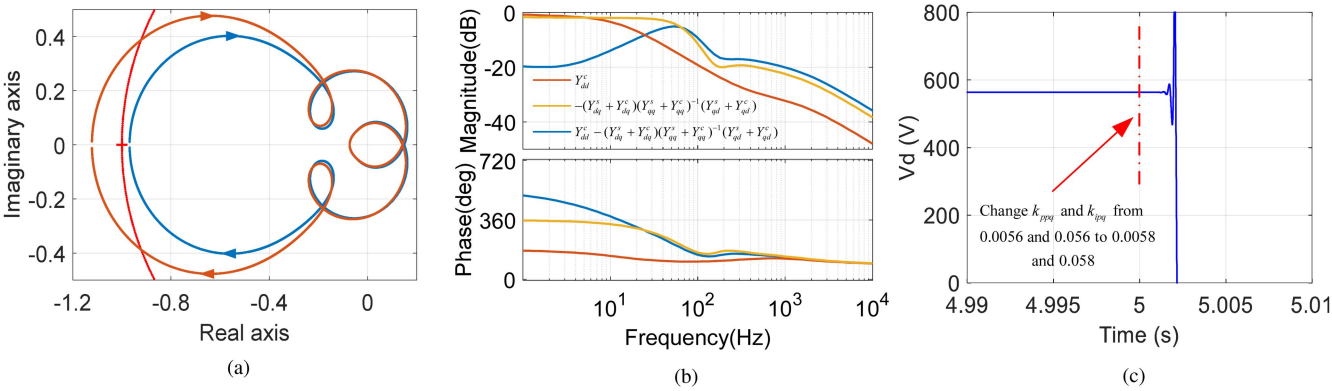

Fig. 9. Case study of the grid-connected converter operating under PF = 0.9. (a) Nyquist plots of $L'(s)$. (b) Bode diagrams of different admittances. (c) Simulation of the d-axis voltage v_d in the time domain.

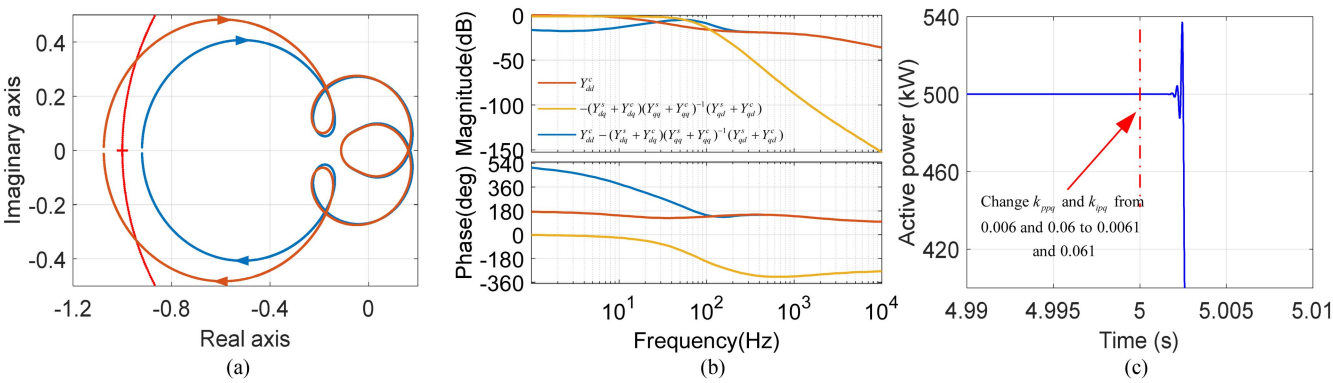

Fig. 10. Case study of the grid-connected converter operating under PF = 1. (a) Nyquist plots of $L'(s)$. (b) Bode diagrams of different admittances. (c) Simulation of the active power in the time domain.

now contains one RHP pole and becomes unstable, agreeing with the time-domain waveform of the active power shown in Fig. 8(c). With respect to Fig. 8(c), when the bandwidth of the power control loop is increased at $t = 5$ s, the active power deviates from its reference value and the system gets out of control rapidly. Furthermore, since the magnitude of $-(Y^s_{dq} + Y^c_{dq})(Y^s_{qq} + Y^c_{qq})^{-1}(Y^s_{qd} + Y^c_{qd})$ shown in Fig. 8(b) is larger than that of Y^c_{dd} around 6000 Hz, the system instability is triggered by the coupling of the d-axis subsystem with the q-axis subsystem instead of the d-axis converter admittance. The analysis result of the converter operating under PF = 0.9 is presented in Fig. 9. Since it has a similar condition with the converter operating under PF = 0.8, to avoid repetition, the detailed discussion is neglected here.

Fig. 10 demonstrates the analysis result of the converter operating under PF = 1. As illustrated by Fig. 10(a), before the parameter change, the Nyquist plot of $L'(s)$ marked by blue color does not surround $(-1, j0)$ point and the system keeps stable. On the contrary, subsequent to the bandwidth increase of the power control loop, the Nyquist plot of $L'(s)$ marked by orange color surrounds $(-1, j0)$ point once clockwise. Therefore, the system contains one RHP pole and gets out of control. Fig. 10(c) presents the time-domain simulation of the active power. As shown in Fig. 10(c), the system becomes unstable with the change of k_{ppq} and k_{ipq}, which means $L'(s)$ accurately predict the system stability condition. Notice that the Nyquist plot marked by orange color interacts with the unit circle at 6000 Hz. To investigate the system instability root cause, the different Bode diagrams in Fig. 10(b) are compared around 6000 Hz. Since the magnitude of Y_{dd}^c is much larger than that of $-(Y_{dq}^s + Y_{dq}^c)(Y_{qq}^s + Y_{qq}^c)^{-1}(Y_{qd}^s + Y_{qd}^c)$, for the converter operating under PF = 1, the d-axis converter admittance instead of the coupling of the d-axis subsystem with the q-axis subsystem accounts for the system instability.

V. Conclusion

This article formulates a sequential SISO stability analysis model for grid-connected converter systems. Compared with the existing SISO models, the one established in this article features a more clear physical meaning and explicitly identifies the impact of different parts on system stability. Furthermore, the proposed sequential SISO stability analysis model never includes any RHP pole. As a bonus, the system stability can be judged intuitively from impedance interactions just like the dc systems. The classical control theory can also be easily introduced to guide the system analysis and design.

References

[1] F. Blaabjerg, Z. Chen, and S. B. Kjaer, "Power electronics as efficient interface in dispersed power generation systems," *IEEE Trans. Power Electron.*, vol. 19, no. 5, pp. 1184–1194, Sep. 2004.

[2] J. M. Carrasco et al., "Power-electronic systems for the grid integration of renewable energy sources: A survey," *IEEE Trans. Ind. Electron.*, vol. 53, no. 4, pp. 1002–1016, Jun. 2006.

[3] M. H. Ali, B. Wu, and R. A. Dougal, "An overview of SMES applications in power and energy systems," *IEEE Trans. Sustain. Energy*, vol. 1, no. 1, pp. 38–47, Apr. 2010.

[4] H. Liu, X. Xie, and W. Liu, "An oscillatory stability criterion based on the unified dq-frame impedance network model for power systems with high-penetration renewables," *IEEE Trans. Power Syst.*, vol. 33, no. 3, pp. 3472–3485, May 2018.

[5] H. Liu and X. Xie, "Comparative studies on the impedance models of VSC-based renewable generators for SSI stability analysis," *IEEE Trans. Energy Convers.*, vol. 34, no. 3, pp. 1442–1453, Sep. 2019.

[6] R. D. Middlebrook, "Input filter considerations in design and application of switching regulators," in *Proc. IEEE Ind. Appl. Soc. Annu. Meeting*, 1976, pp. 366–382.

[7] M. Belkhayat, "Stability criteria for AC power systems with regulated loads," Ph.D. dissertation, Purdue Univ., West Lafayette, NI, USA, 1997.

[8] X. Wang and F. Blaabjerg, "Harmonic stability in power electronic based power systems: Concept, modeling, and analysis," *IEEE Trans. Smart Grid*, vol. 10, no. 3, pp. 2858–2870, May 2019.

[9] P. Kundur, N. J. Balu, and M. G. Lauby, *Power System Stability and Control*, vol. 7. New York, NY, USA: McGraw-hill, 1994.

[10] X.-F. Wang, Y. Song, and M. Irving, *Modern Power Systems Analysis*, vol. 1. Berlin, Germany: Springer, 2010.

[11] S. Skogestad and I. Postlethwaite, *Multivariable Feedback Control: Analysis and Design*, vol. 2. New York, NY, USA: Wiley, 2007.

[12] L. Fan and Z. Miao, "Admittance-based stability analysis: Bode plots, Nyquist diagrams or eigenvalue analysis?," *IEEE Trans. Power Syst.*, vol. 35, no. 4, pp. 3312–3315, Jul. 2020.

[13] M. Amin and M. Molinas, "Small-signal stability assessment of power electronics based power systems: A discussion of impedance-and eigenvalue-based methods," *IEEE Trans. Ind. Appl.*, vol. 53, no. 5, pp. 5014–5030, Sep./Oct. 2017.

[14] H. Zhang, M. Mehrabankhomartash, M. Saeedifard, Y. Zou, Y. Meng, and X. Wang, "Impedance analysis and stabilization of point-to-point HVDC systems based on a hybrid AC–DC impedance model," *IEEE Trans. Ind. Electron.*, vol. 68, no. 4, pp. 3224–3238, Apr. 2021.

[15] B. Wen, D. Boroyevich, R. Burgos, P. Mattavelli, and Z. Shen, "Analysis of DQ small-signal impedance of grid-tied inverters," *IEEE Trans. Power Electron.*, vol. 31, no. 1, pp. 675–687, Jan. 2016.

[16] B. Wen, D. Boroyevich, R. Burgos, P. Mattavelli, and Z. Shen, "Small-signal stability analysis of three-phase AC systems in the presence of constant power loads based on measured D-Q frame impedances," *IEEE Trans. Power Electron.*, vol. 30, no. 10, pp. 5952–5963, Oct. 2015.

[17] J. Sun, G. Wang, X. Du, and H. Wang, "A theory for harmonics created by resonance in converter-grid systems," *IEEE Trans. Power Electron.*, vol. 34, no. 4, pp. 3025–3029, Apr. 2019.

[18] J. Sun, Z. Bing, and K. J. Karimi, "Input impedance modeling of multipulse rectifiers by harmonic linearization," *IEEE Trans. Power Electron.*, vol. 24, no. 12, pp. 2812–2820, Dec. 2009.

[19] M. Cespedes and J. Sun, "Impedance modeling and analysis of grid-connected voltage-source converters," *IEEE Trans. Power Electron.*, vol. 29, no. 3, pp. 1254–1261, Mar. 2014.

[20] L. Xu, H. Xin, L. Huang, H. Yuan, P. Ju, and D. Wu, "Symmetric admittance modeling for stability analysis of grid-connected converters," *IEEE Trans. Energy Convers.*, vol. 35, no. 1, pp. 434–444, Mar. 2020.

[21] X. Wang, L. Harnefors, and F. Blaabjerg, "Unified impedance model of grid-connected voltage-source converters," *IEEE Trans. Power Electron.*, vol. 33, no. 2, pp. 1775–1787, Feb. 2018.

[22] M. K. Bakhshizadeh et al., "Couplings in phase domain impedance modeling of grid-connected converters," *IEEE Trans. Power Electron.*, vol. 31, no. 10, pp. 6792–6796, Oct. 2016.

[23] W. Liu, X. Xie, X. Zhang, and X. Li, "Frequency-coupling admittance modeling of converter-based wind turbine generators and the control-hardware-in-the-loop validation," *IEEE Trans. Energy Convers.*, vol. 35, no. 1, pp. 425–433, Mar. 2020.

[24] J. Sun, "Impedance-based stability criterion for grid-connected inverters," *IEEE Trans. Power Electron.*, vol. 26, no. 11, pp. 3075–3078, Nov. 2011.

[25] B. Wen, D. Boroyevich, R. Burgos, P. Mattavelli, and Z. Shen, "Inverse Nyquist stability criterion for grid-tied inverters," *IEEE Trans. Power Electron.*, vol. 32, no. 2, pp. 1548–1556, Feb. 2017.

[26] C. Zhang, X. Cai, A. Rygg, and M. Molinas, "Sequence domain SISO equivalent models of a grid-tied voltage source converter system for small-signal stability analysis," *IEEE Trans. Energy Convers.*, vol. 33, no. 2, pp. 741–749, Jun. 2018.

[27] S. Shah, P. Koralewicz, V. Gevorgian, and R. Wallen, "Sequence impedance measurement of utility-scale wind turbines and inverters reference frame, frequency coupling, and MIMO/SISO forms," *IEEE Trans. Energy Convers.*, vol. 37, no. 1, pp. 75–86, Mar. 2022.

[28] X. Meng et al., "Conversion and SISO equivalence of impedance model of single-phase converter in electric multiple units," *IEEE Trans. Transp. Electrific.*, vol. 9, no. 1, pp. 1363–1378, Mar. 2023.

[29] C. Yang, H. Xin, Z. Gong, W. Dong, P. Ju, and L. Xu, "Complex circuit analysis and investigation on applicability of generalized-impedance-based stability criterion for grid-connected converter," *Proc. CSEE*, vol. 40, no. 15, pp. 4744–4757, 2020.

[30] C. Zhang, M. Molinas, S. Føyen, J. A. Suul, and T. Isobe, "Harmonic-domain SISO equivalent impedance modeling and stability analysis of a single-phase grid-connected VSC," *IEEE Trans. Power Electron.*, vol. 35, no. 9, pp. 9770–9783, Sep. 2020.

[31] Z. Li, M. Zhu, C. Hou, H. Wang, Y. Li, and X. Cai, "Impedance modelling mechanisms and stability issues of single phase inverter with SISO structure and frequency coupling effect," *IEEE Trans. Energy Convers.*, vol. 37, no. 1, pp. 573–584, Mar. 2022.

[32] J. Lin, M. Su, Y. Sun, S. Xie, W. Xiong, and X. Li, "Unified SISO loop gain modeling, measurement, and stability analysis of three-phase voltage source converters," *IEEE Trans. Energy Convers.*, vol. 37, no. 3, pp. 1907–1920, Sep. 2022.

[33] H. Zhang, L. Harnefors, X. Wang, H. Gong, and J.-P. Hasler, "Stability analysis of grid-connected voltage-source converters using SISO modeling," *IEEE Trans. Power Electron.*, vol. 34, no. 8, pp. 8104–8117, Aug. 2019.

[34] H. Zhang, X. Wang, L. Harnefors, H. Gong, J.-P. Hasler, and H.-P. Nee, "SISO transfer functions for stability analysis of grid-connected voltage-source converters," *IEEE Trans. Ind. Appl.*, vol. 55, no. 3, pp. 2931–2941, May/Jun. 2019.

[35] L. Harnefors, X. Wang, S.-F. Chou, M. Bongiorno, M. Hinkkanen, and M. Routimo, "Asymmetric complex-vector models with application to VSC–grid interaction," *IEEE Trans. Emerg. Sel. Topics Power Electron.*, vol. 8, no. 2, pp. 1911–1921, Jun. 2020.

[36] J. Guo et al., "Harmonic transfer-function-based $\alpha\beta$-frame SISO impedance modeling of droop inverters-based islanded microgrid with unbalanced loads," *IEEE Trans. Ind. Electron.*, vol. 70, no. 1, pp. 452–464, Jan. 2023.

[37] C. Guo, S. Yang, W. Liu, C. Zhao, and J. Hu, "Small-signal stability enhancement approach for VSC-HVDC system under weak ac grid conditions based on single-input single-output transfer function model," *IEEE Trans. Power Del.*, vol. 36, no. 3, pp. 1313–1323, Jun. 2021.

[38] J. Yu, S. Wang, Z. Liu, J. Li, J. Liu, and J. Shang, "Accurate small-signal terminal characteristic model and SISO stability analysis approach for parallel grid-forming inverters in islanded microgrids," *IEEE Trans. Power Electron.*, vol. 38, no. 5, pp. 6597–6612, May 2023.

[39] D. Yang and Y. Sun, "SISO impedance-based stability analysis for system-level small-signal stability assessment of large-scale power electronics-dominated power systems," *IEEE Trans. Sustain. Energy*, vol. 13, no. 1, pp. 537–550, Jan. 2022.

[40] J. Lin, M. Su, Y. Sun, D. Yang, and S. Xie, "Recursive SISO impedance modeling of single-phase voltage source rectifiers," *IEEE Trans. Power Electron.*, vol. 37, no. 2, pp. 1296–1309, Feb. 2022.

[41] X. Tang, Z. Li, W. Wang, L. Liu, B. Qu, and J. M. Guerrero, "A decoupling control method for converting DIDO sequence admittance model of grid-tied converter system into SISO," *IEEE Trans. Energy Convers.*, vol. 38, no. 4, pp. 2647–2661, Dec. 2023.

[42] S. Li, Y. Yan, and X. Yuan, "SISO equivalent of MIMO VSC–dominated power systems for voltage amplitude and phase dynamic analyses in current control timescale," *IEEE Trans. Energy Convers.*, vol. 34, no. 3, pp. 1454–1465, Sep. 2019.

[43] M. Amin and Q.-C. Zhong, "Impedance modeling and stability analysis of grid-tied universal droop control inverter," in *Proc. IEEE Energy Convers. Congr. Expo.*, 2019, pp. 5569–5575.

[44] J. Guo et al., "Impedance analysis and stabilization of virtual synchronous generators with different dc-link voltage controllers under weak grid," *IEEE Trans. Power Electron.*, vol. 36, no. 10, pp. 11397–11408, Oct. 2021.